

Dynamical Evolution of Simulated Particles Ejected from Asteroid Bennu

Jay W. McMahon¹, Daniel J. Scheeres¹, Steven R. Chesley², Andrew French¹,
Daniel Brack¹, Davide Farnocchia², Yu Takahashi², Benjamin Rozitis⁷,
Pasquale Tricarico³, Erwan Mazarico⁴, Beau Bierhaus⁵, Joshua P. Emery⁸,
Carl W. Hergenrother⁶, Dante S. Laretta⁶

¹Smead Aerospace Engineering Sciences Department, University of Colorado, Boulder, Colorado

²Jet Propulsion Laboratory, California Institute of Technology, Pasadena, California

³Planetary Science Institute, Tucson, Arizona

⁴NASA Goddard Space Flight Center, Greenbelt, Maryland

⁵Lockheed Martin Space, Littleton, Colorado

⁶Lunar and Planetary Laboratory, University of Arizona, Tucson, Arizona

⁷School of Physical Sciences, The Open University, Milton Keynes, UK

⁸Department of Earth and Planetary Sciences, University of Tennessee, Knoxville, TN, USA

Key Points:

- Ejected particles from the surface of Bennu can survive for periods of days to years at a range of altitudes above the asteroid.
- Ejected small particles are preferentially removed from system, which could cause a deficit of small particles on the surface.
- Particles that return to the surface preferentially land at low latitudes, which can in-fill craters and grow the equatorial bulge without requiring landslides.

Abstract

In early 2019, the OSIRIS-REx spacecraft discovered small particles being ejected from the surface of the near-Earth asteroid Bennu. Although they were seen to be ejected at slow speeds, on the order of tens of cm/s, a number of particles were surprisingly seen to orbit for multiple revolutions and days, which requires a dynamical mechanism to quickly and substantially modify the orbit to prevent re-impact upon their first periaipse passage. This paper demonstrates that, based on simulations constrained by the conditions of the observed events, the combined effects of gravity, solar radiation pressure, and thermal radiation pressure from Bennu can produce many sustained orbits for ejected particles. Furthermore, the simulated populations exhibit two interesting phenomena that could play an important role in the geophysical evolution of bodies such as Bennu. First, small particles (< 1 cm radius) are preferentially removed from the system, which could lead to a deficit of such particles on the surface. Second, re-impacting particles preferentially land near or on the equatorial bulge of Bennu. Over time, this can lead to crater in-filling and growth of the equatorial radius without requiring landslides.

1 Introduction

The OSIRIS-REx spacecraft arrived at the near-Earth asteroid Bennu in late 2018 (D. Lauretta et al., 2019). In early 2019, particles were discovered being ejected from the surface of Bennu (D. S. Lauretta et al., 2019; Hergenrother et al., 2019). One surprise was the length of the lifetimes of several of the observed particles, whose orbits were estimated to last multiple days and complete many revolutions (D. S. Lauretta et al., 2019) — demonstrating that some fraction of the ejected particles were put into orbits that neither immediately re-impacted the surface nor immediately escaped the system. These observations brought up many questions. What dynamical processes could lead to such orbits? How do particles launched at relatively slow speeds avoid the fate of re-impacting the surface as they come back down toward their first periaipse passage? How long can ejected particles stay in orbit around Bennu? When ejected particles do re-impact, where do they land? This paper addresses these questions.

Bennu is a small near-Earth asteroid, approximately 500 m in diameter, with a rubble-pile structure, a rocky surface, and a “top” shaped profile with an equatorial bulge (D. Lauretta et al., 2019; Scheeres et al., 2019; DellaGiustina et al., 2019; Barnouin et al., 2019). The dynamical environment of Bennu is complex due to the low gravity and non-spherical shape of this small body (Scheeres et al., 2019). This means that orbits in proximity of the body are highly perturbed by solar radiation pressure (SRP) forces and are non-Keplerian and rapidly evolving in general (Scheeres, 2016).

Most studies of orbits about small asteroids focus on stable orbits that will be useful for spacecraft exploring such bodies. Scheeres (2016) has developed an averaged theory that succinctly describes the evolution of orbits around small bodies when they are perturbed by SRP. He shows the existence of frozen orbits and stable terminator orbits, which have now been successfully flown by the OSIRIS-REx spacecraft (Leonard et al., 2019). Many studies have advanced this work, finding specific types of orbits that exist under the SRP and solar gravity perturbations, including quasi-terminator orbits (Broschart et al., 2014), heliotropic orbits (Lantukh et al., 2015; Russell et al., 2016) and resonant terminator orbits (Broschart et al., 2009). More recent work motivated by the OSIRIS-REx mission studied the long-term stability of theoretical small moons in the vicinity of Bennu (Rieger et al., 2018). All of these studies provide insight into the dynamical processes in orbit, but do not focus on how material could leave the surface to reach these orbits.

The leading hypotheses for the cause of the observed ejection events at Bennu are thermal fracturing or micrometeorite impacts, either of which could lead to the relatively

low energy ejecta seen at Bennu (D. S. Lauretta et al., 2019). There has been a significant amount of work investigating ejecta from natural and man-made impacts on small asteroids. Unfortunately, these impacts take place at high-energies, meaning that much of the ejecta is at higher speeds than is of concern here. However, a few studies have looked at the low-velocity portion of the ejecta population. The understanding of the fate of impact ejecta at asteroids is discussed by Scheeres et al. (2002), which points out how ejecta at small asteroids can, in theory, enter into orbits under the effects of gravity and SRP. Specific studies of ejecta at Ida (Geissler et al., 1996) and Eros (Korycansky & Asphaug, 2004) provide interesting comparisons to the current case; however, those bodies are an order of magnitude larger than Bennu and the dynamics are therefore more strongly dominated by gravity. Furthermore, statistical results from those studies would not directly apply here because they are conditioned on initial ejecta populations created from high-energy impacts.

Similarly, there have been studies of the fate of ejecta and debris from man-made impacts on asteroids. In particular, studies of the expected evolution of the debris cloud after the impact of the DART mission (Yu et al., 2017; Yu & Michel, 2018; Schwartz et al., 2016) and the Hayabusa2 Small Carryon Impactor experiment (Giancotti et al., 2014; Arakawa et al., 2017) have been carried out recently. While these asteroids are more similar in size to Bennu, the source of the ejecta is again from a high-energy impact, which differs from the observed events at Bennu because they predominantly produce high-velocity ejecta that quickly escape the system.

A recent study by Vetrivano et al. (2016) has provided the closest study of low-speed ejecta from a small body to predict the events at Bennu. The fate of the ejecta is strongly controlled by the effects of SRP, which has also been found by Garcia Yarnoz et al. (2014). While these works are relevant and provide valuable insight, it is crucial to include two other effects to get realistic results, especially for low-altitude particles: shadowing from the primary body which turns off SRP when eclipsed (Russell et al., 2016), and thermal radiation pressure forces from the infrared radiation leaving Bennu (Hesar et al., 2017).

This paper investigates the evolutionary outcomes of populations of simulated particles ejected from the surface under conditions similar to those observed at Bennu. Such an analysis provides insight into how ejection events can influence the distribution of material over the surface of the asteroid. The results presented here are constrained by the ejection events observed in early 2019 (D. S. Lauretta et al., 2019; Hergenrother et al., 2019). The estimated ejection locations, timing, and velocity ranges from D. S. Lauretta et al. (2019) are used in this paper, as well as representative particle sizes and masses that encompass the best available data. Having said that, the point of this paper is not to produce true or estimated orbits; based on our knowledge of the particle dynamics and Bennu’s properties, that can only be done reliably with trajectories estimated from observations (D. S. Lauretta et al., 2019). Rather, this paper explores the influence of the parameters of the dynamical system and the particle initial conditions to understand the larger issues regarding how particles could move around in this system. We seek to balance the accuracy of the dynamics with computational speed, given the uncertainties still in the models (e.g. from gravity, albedo, unmodeled dynamics), to keep computational speed tractable such that we can produce large numbers of simulations to understand the trends within a population of ejected particles. Thus, the real value in the results presented here is in the range of behaviors that can result from an ejection event. The population evolution that we simulate indicates that if ejection events occur often enough, they can play an important role in the geophysical properties of Bennu.

2 Dynamic Modeling

Effects that are typically thought of as small perturbations from the perspective of classical astrodynamics around planets become extremely important around small bod-

ies owing to the weak gravity. The dynamics considered in this work are shape model-based gravity, solar tides, SRP including shadowing, and shape model-based thermal/albedo radiation pressure. In the course of this work and previous studies, it is found that all of these dynamics are crucial to producing the correct evolutionary behavior for the ejected particles. Each of the dynamic models are discussed in turn in the following sections.

2.1 Gravity

Although small, the main source of orbital dynamics is still the gravitational forces caused by the asteroid. We use the constant density polyhedral gravity model (Werner & Scheeres, 1996) to simulate the gravity field from the v20 Benu shape model constructed from data obtained by the OSIRIS-REx spacecraft (Barnouin et al., 2019) and the estimated Benu density of 1.19 g/cc (Scheeres et al., 2019). Particular parameters used for these models are given in Section 4.

The top shape of Benu produces a gravity field that is primarily dominated by the even zonal harmonics, especially J_2 and J_4 (McMahon et al., 2018). The body is relatively symmetric at a global scale with respect to the pole and the equator (Barnouin et al., 2019), meaning that the odd zonal and tesseral harmonics are less significant, but do exist and are captured by the polyhedral gravity model. Because Benu does not exhibit any significant wobble in its rotational pole (D. Lauretta et al., 2019; Barnouin et al., 2019), the main effect of the non-spherical gravity potential is to precess a particle orbit's angular momentum and eccentricity vectors (Scheeres, 2016).

The other important gravitational effect which must be considered is the effect of solar tides, which are modeled as

$$\mathbf{a}_{3rd} = \mu_{Sun} \left[\frac{\mathbf{r}_{Sun/p}}{|\mathbf{r}_{Sun/p}|^3} - \frac{\mathbf{r}_{Sun/Ast}}{|\mathbf{r}_{Sun/Ast}|^3} \right] \quad (1)$$

where μ_{Sun} is the gravitational parameter of the Sun, $\mathbf{r}_{Sun/p}$ is the vector pointing from the particle to the Sun, and $\mathbf{r}_{Sun/Ast}$ is the vector pointing from the center of the asteroid to the Sun. Solar tides will also primarily have the effect of torquing a particle's orbit to precess the angular momentum and eccentricity vectors. On a longer timescale, the solar tides can lead to the Kozai effect trading inclination and eccentricity for non-equatorial orbits (Rieger et al., 2018); however, this secular effect is often interrupted for the particles considered in this work given the rapid evolution of orbits from the other dynamics acting in the system.

2.2 Solar Radiation Pressure

After gravity, SRP is the most important force acting on the ejected particles. The most widely used model for SRP is the so-called cannonball model, which captures the primary component of the acceleration in the anti-Sun direction. The particular version of the SRP model used here is shown in Eq. 2.

$$\mathbf{a}_{SRP} = -H(\mathbf{r}) \frac{P_0}{|\mathbf{r}_{Sun/Ast}|^2} \left(1 + \frac{4}{9}\rho \right) \frac{A}{m} \hat{\mathbf{r}}_{Sun/Ast} \quad (2)$$

where $H(\mathbf{r})$ is the shadowing function that takes a value of 0 if the particle is positioned (where \mathbf{r} is the particle's position with respect to the asteroid) behind Benu such that the Sun is occulted, and 1 otherwise. We do not model any partial shadowing/penumbra effects. In our code, and as shown in Eq. 2 we approximate the distance from the Sun to the particle as $|\mathbf{r}_{Sun/Ast}|$, as the difference between these is minimal. The same is true for $\hat{\mathbf{r}}_{Sun/Ast}$, which is the unit vector from Benu (as opposed to the particle) to the Sun.

164 The minus sign makes the SRP acceleration act in the anti-Sun direction. P_0 is the so-
 165 lar pressure constant, which has a value of 1×10^{14} kg km/s², ρ is the reflectivity, or
 166 albedo, of the particles, and A/m is the area-to-mass ratio. The simulations only use these
 167 values in ratio, although we do define the individual values from an assumed spherical
 168 shape of constant density (see Section 4). The 4/9 factor that appears with the reflect-
 169 tivity comes from the assumption that the particle is a sphere (on average) that reflects
 170 light in a diffuse Lambertian pattern.

171 It is important to understand the assumptions that are embedded in using this model
 172 for SRP. The name cannonball implies that the particles are spherical. This assumption
 173 is commonly used because an object of any shape, if it is tumbling, will experience an
 174 SRP acceleration away from the Sun on average. Specifically, if an object is tumbling
 175 such that 1) its rotational rate is much faster than the mean motion of the orbit, and
 176 2) there is an equal probability of the body being at any inertial attitude in time, then
 177 the SRP model will average out to being in the anti-Sun direction. The interpretation
 178 of the area-to-mass ratio being from a spherical particle of constant density is an easy
 179 way to compute realistic and representative area-to-mass ratios. Because the particles
 180 in reality could be closer to a tumbling plate-like shape (Rizk et al., 2019), the relation-
 181 ship of area-to-mass ratio to density and reflectivity should be taken with some uncer-
 182 tainty as it is an averaged dynamical quantity. Two further assumptions are embedded
 183 in this model: 1) any reflected light is reflected in a purely diffuse Lambertian manner;
 184 2) absorbed light that is re-emitted as infrared radiation cause any acceleration on the
 185 body because the small sizes and assumed tumbling motion leads to the particles being
 186 isothermal.

187 In order to produce realistic orbital evolution, it is crucial to include shadowing as
 188 represented by the $H(\mathbf{r})$. This fundamentally changes the effects of SRP on an orbit. For
 189 example, without shadowing, SRP on average does not change the semimajor axis of the
 190 orbit. However, when shadowing is taken into account a change of semimajor axis can
 191 occur. The details of our implementation of a fast shadowing algorithm are discussed
 192 in Section 3.

193 2.3 Thermal Radiation Pressure

194 Thermal radiation pressure (TRP) from the radiation emanating from the aster-
 195 oid is generally much smaller than SRP. However, in this scenario, all particles neces-
 196 sarily spend time near the surface, where the TRP forces can approach or even exceed
 197 SRP. Therefore it is crucial to include these forces in the dynamical models simulated.

198 The TRP model used is from Hesar et al. (2017), but simplified for a cannonball
 199 particle instead of a complex spacecraft shape as in that work. The acceleration can be
 200 computed as

$$201 \mathbf{a}_{th} = -\frac{(1 + \alpha)A}{m} \sum_{i \in F}^{N_F} P_i \frac{(\mathbf{r} - \mathbf{r}_i)}{|\mathbf{r} - \mathbf{r}_i|} \quad (3)$$

202 where the summation goes over the number of facets of the shape model, N_F , whose po-
 203 sitions are referenced on the body by the position of their centers, \mathbf{r}_i . There can be a
 204 reflection of the incident radiation based on an infrared albedo, α ; however, we treat this
 205 parameter as zero in this work given the isothermal assumption discussed in Section 2.2.
 P_i is the infrared pressure coming from facet i , which is defined as

$$206 P_i = (\tau \rho_{Ast} G_R \cos \Theta + \epsilon \sigma_B T_i^4) \frac{\cos \phi A_i}{c \pi |\mathbf{r} - \mathbf{r}_i|^2} \quad (4)$$

206 where τ_i is the visibility function of the surface element i with respect to the sunlight;
 207 that is, τ_i is equal to 1 if that surface element is lit by the sunlight and 0 otherwise. Θ
 208 is the angle between the facet normal and the incident sunlight. ρ_{Ast} is the albedo of Benu,
 209 which is defined as the fraction of the shortwave radiation reflected from the surface of
 210 the body to the incident shortwave solar radiation. Here we assume a constant albedo
 211 across the entire surface of the body of 4% (Hergenrother et al., 2019). G_R is the solar
 212 flux at the distance $R = |\mathbf{r}_{Sun/Ast}|$ from the Sun ($= 1368 \text{ J s}^{-1} \text{ m}^2$ at 1AU) and c is
 213 the speed of light. A_i is the surface area of facet i . ϕ is the angle between the facet nor-
 214 mal and the vector connecting the particle and the facet center. This determines the vis-
 215 ibility, and if $\phi < 0$, this facet does not contribute to the total TRP at this time. ϵ is
 216 the surface emissivity of Benu, and σ_B is the Stefan Boltzmann constant.

217 T_i is the temperature of the facet, which is determined by the Advanced Thermo-
 218 physical Model (ATPM) of Rozitis and Green (2011, 2012, 2013) using the thermophys-
 219 ical properties of Benu derived by DellaGiustina et al. (2019). The hottest region on
 220 the asteroid is in the mid-afternoon. The ATPM takes into account topography and ther-
 221 mal inertia effects such that the temperatures are not symmetric, and the TRP accel-
 222 eration at a given location will vary with the spin state of Benu. This variation shrinks
 223 as altitude increases such that it is insignificant by around 1 km, but at low altitudes
 224 the variation can be 5 to 10% of the total TRP. The temperature map is computed at
 225 one specific Benu orbit distance, so that the temperature used is scaled by the relation-
 226 ship

$$T_i^4 = \frac{R_0^2}{R^2} T_{i,0}^4 \quad (5)$$

227 where R_0 and $T_{i,0}$ are the distance to the Sun and the facet temperature at the epoch
 228 location, respectively. As with the SRP model, this model assumes that the particle is
 229 rapidly rotating such that its area-to-mass ratio averages to an effective constant value
 230 represented by the sphere in this work. The final term in Eq. 4 becomes extremely large
 231 as a particle approaches the surface such that $|\mathbf{r} - \mathbf{r}_i| \rightarrow 0$. This is not physical, but
 232 rather is an artifact of the discretization of the asteroid surface with finite facets. Thus
 233 we implement a limit in our simulations such that $A_i/|\mathbf{r} - \mathbf{r}_i|$ can never be larger than
 234 1. Although this is not physically exact, it captures the main behavior without requir-
 235 ing us to switch to a higher-resolution shape and temperature map, which would not sig-
 236 nificantly change the results.

237 3 Numerical Methods

238 The main simulation is written in Matlab, using the variable-step Runge-Kutta 45
 239 integrator `ode45`. This integrator performed well in this scenario once a normalization
 240 scheme was implemented to improve the numerics. The normalizing length is chosen to
 241 be the minimum radius of the shape model used, $\bar{r} = 214.68 \text{ m}$. This has the effect that
 242 a normalized position vector of length < 1 is guaranteed to be inside the body. The nor-
 243 malizing time is then computed based on the mean motion at this distance, which is $\bar{t} =$
 244 $\sqrt{\bar{r}^3/\mu} = 1421.51 \text{ s}$, and the associated normalizing velocity is computed as the circu-
 245 lar speed at the reference length, which is then $\bar{v} = \sqrt{\mu/\bar{r}} = 15.1 \text{ cm/s}$. This results
 246 in a normalized $\mu = 1$. Using this normalization scheme allows us to use reasonable tol-
 247 erances: a relative tolerance of 1×10^{-3} and an absolute tolerance of 1×10^{-6} .

248 Several other important components of the simulation implementation allow for fast
 249 execution. The polyhedral gravity mode, which is by far the most computationally com-
 250 plex portion of the dynamics, is coded in C and interfaced through a MEX function. The
 251 TRP model is written in Matlab, but is formulated to take advantage of Matlab's sparse
 252 matrix capabilities to speed up the dot products that are computed for every facet of
 253 the shape model, which has produced a significant speed increase.

254 Finally, the shadowing model can be another computational bottleneck if ray-tracing
 255 is used. To avoid this, the shadowing algorithm is based on approximate limbs of Bennu
 256 represented by a convex hull defined by the maximum radius at every 12 degrees of lat-
 257 itude. This can then be represented with 30 pie-shaped triangular facets connected to
 258 the center of the shape model. This set of facets is used to check for shadowing and/or
 259 re-impact by projecting a particle’s position vector onto the terminator plane and test-
 260 ing whether it resides within any of these facets; if so, then it can be determined whether
 261 it is in shadow or has impacted the body by looking at the total radius and comparing
 262 to the limb radius at that latitude. Our testing has shown that, while this approxima-
 263 tion may be too rough for fitting precise measurement data, the dynamics produced do
 264 not differ meaningfully from a more precise model, and so the general trends presented
 265 in this work do not change substantially.

266 4 Ejection Event Simulation Parameters

267 The simulation results presented here are constrained by the measured quantities
 268 of Bennu and the particle ejection events. We investigate the evolution of particles based
 269 on the first three largest observed ejection events, which occurred on January 6, January
 270 19, and February 11, 2019 (D. S. Lauretta et al., 2019). Various parameters used in the
 271 simulations are given in Table 1. The second and third events have well estimated ejec-
 272 tion locations on the body, which are used here. The January 6 event, however, has some
 273 uncertainty in the ejection location, which results in two possible ejection locations, which
 274 are referred to as Site A and Site B in this work (near and far solutions, respectively, in
 275 D. S. Lauretta et al. (2019)). Thus we simulate four ejection events, one for each site/date
 276 combination as shown in Table 1.

277 In this work the v20 shape model of Barnouin et al. (2019) was downsampled to
 278 a vertex spacing resolution of approximately 12.58-m with 12288 facets and 6534 ver-
 279 tices, which provides a good balance between accuracy for topography and gravity for
 280 a reasonable computational load. The radius for each event location in Table 1 is com-
 281 puted from where the indicated latitude and longitude intersect this shape model, so these
 282 values may differ slightly from reality at that location. The temperature model uses the
 283 same shape model resolution but is updated from the v13 shape model used in DellaGiustina
 284 et al. (2019) to the v20 shape model used here.

285 We made some approximations and assumptions to simplify certain aspects of the
 286 simulation without sacrificing the understanding of the general behavior of the ejected
 287 particles. First, particles are all modeled with reflectivity $\rho = 0.04$, which is the mean
 288 Bennu albedo. Particles are modeled as spheres, such that the area-to-mass ratio varies
 289 as

$$\frac{A}{m} = \frac{3}{4} \frac{1}{d_p r_{part}} \quad (6)$$

290 where d_p is the particle density and r_{part} is particle radius. In this work we used an as-
 291 sumed constant particle density of $d_p = 2 \text{ g/cm}^3$ which is similar to Bennu’s bulk den-
 292 sity and consistent with meteorite analogs (D. Lauretta et al., 2019; Hamilton et al., 2019).
 293 This value is within the range of densities found in D. S. Lauretta et al. (2019), however
 294 as discussed in Section 2, the area-to-mass ratio controls the SRP and TRP accelerations,
 295 thus trading density and particle size can result in equivalent trajectories for different
 296 particle models. The SRP acceleration is also modified by the $(4/9)\rho$ term in Eq. 2, which
 297 means that changing the reflectivity will also influence the dynamics, albeit with a weaker
 298 effect than the area-to-mass ratio. Overall these values are based on the best informa-
 299 tion to date, but the population explored covers a range of area-to-mass ratios to try to
 300 encompass any expected variation.

Table 1. Parameters used in simulation studies. Obtained from (D. S. Lauretta et al., 2019) except where noted otherwise.

| | Parameter | Value |
|---------------|---------------------|--|
| Jan 6, Site A | Radius ^a | 238.89 m |
| | Latitude | -74.95° |
| | Longitude | 325.32° |
| | Local time | 15:22 |
| Jan 6, Site B | Radius | 236.61 m |
| | Latitude | -57.30° |
| | Longitude | 343.67° |
| | Local time | 16:35 |
| Jan 19 | Radius | 247.51 m |
| | Latitude | 20.63° |
| | Longitude | 335.40° |
| | Local time | 16:38 |
| Feb 11 | Radius | 246.41 m |
| | Latitude | 20.68° |
| | Longitude | 60.17° |
| | Local time | 18:05 |
| Bennu | μ | 4.892 m ³ /s ² (Scheeres et al., 2019) |
| | Pole obliquity | 180° |
| | Spin period | 4.297461 hours |
| | Temperature Map | ATPM (Rozitis & Green, 2011, 2012, 2013; DellaGiustina et al., 2019) |
| | Shape Model | (Barnouin et al., 2019) |
| Particles | Ephemeris | JPL SPK ^b |
| | ρ | 0.04 |
| | Density | 2 g/cc |

^a Radius of the Bennu shape model at the ejection site.^b JPL Small-Body Database Browser: <https://ssd.jpl.nasa.gov/sbdb.cgi>

301 Two other approximations are made to simplify the simulation environment. Bennu’s
 302 spin pole is assumed to be perfectly retrograde with respect to its orbit angular momen-
 303 tum, when in fact there is a small obliquity difference (Barnouin et al., 2019). However,
 304 the maximum error in this assumption is only 2.55° over Bennu’s orbit (determined us-
 305 ing the Bennu ephemeris and estimated pole available from the *OSIRIS-REx NAIF Repos-*
 306 *itory* (2020)), thus this approximation should have only a small effect. Second, as dis-
 307 cussed previously, the gravity is based on a constant density assumption with a finite-
 308 resolution shape model. While there are some indications that there is an inhomogeneous
 309 density distribution (Scheeres et al., 2019), the differences in the gravity field seen so far
 310 indicate that the constant density assumption is a reasonable first approximation, es-
 311 pecially given that we do not know the true density distribution at this point. The same
 312 reasoning indicates that the chosen shape model gives a representative gravity field, es-
 313 pecially at altitudes more than a few meters from the surface.

314 Given the above parameters, there are four degrees of freedom left to sample to sim-
 315 ulate a population of ejected particles: the three dimensions of the launch velocity vec-
 316 tor and the area-to-mass ratio. The launch velocity vector is the initial velocity vector
 317 with respect to the Bennu surface at which a particle is launched. The vector is param-
 318 eterized by the magnitude and two directions: an azimuth angle measured from local East,
 319 and an elevation angle measured from the plane of the shape model facet where the ejec-
 320 tion event is located. The observations of the three ejection events show initial veloc-
 321 ities ranging from 7 to 330 cm/s (D. S. Lauretta et al., 2019). In order to understand
 322 the possible orbital evolutions, we create populations of particles that sample all direc-
 323 tions in the hemisphere above the ejection facet. The azimuth is simulated in discrete
 324 steps of 30° , while the elevation is simulated in steps of 15° . The velocities simulated
 325 range from 10 to 30 cm/s (note that all particles launched faster than 30 cm/s escape
 326 immediately, as shown below), in steps of 2 cm/s. Finally, to explore the area-to-mass
 327 ratio, the particle radius is varied from the set of 0.1, 0.5, and 1 to 20 cm. All told, this
 328 results in a grid of 11 velocities, 7 elevations, 12 azimuths, and 22 particle radii and area-
 329 to-mass ratios for a total of 17,666 simulations from each event/site (the azimuth does
 330 not come into play at an elevation of 90°).

331 Because the particle velocities are sampled from a Bennu-relative grid, the initial
 332 velocity used for simulation must be expressed in the inertial frame:

$$\mathbf{v} = \mathbf{v}_{\text{Launch}} + \boldsymbol{\omega} \times \mathbf{r}_{\text{site}} \quad (7)$$

333 This means that the initial inertial velocity will be skewed with an eastward component
 334 that grows in magnitude for sites closer to the equator of Bennu. Thus, westward (az-
 335 imuth around 180°) cases can have initial inertial velocity magnitudes less than 10 cm/s,
 336 while eastward particles can be greater than 30 cm/s.

337 5 Results

338 Given the set of initial conditions and parameters discussed above, the 17,666 test
 339 particles were simulated for each of the four event times and locations (January 6 Site
 340 A, January 6 Site B, January 19, and February 11). The following sections present some
 341 illustrative orbits to demonstrate the complex dynamical environment with the focus on
 342 understanding the general trends seen within the populations for all of the simulated sce-
 343 narios. In cases where results for one scenario are representative of all simulated scenar-
 344 ios, we show only the results for one.

345

5.1 Orbit Evolution

346

347

348

349

350

351

352

353

354

355

356

The simulated particles demonstrate the rich, complex dynamical environment near Benu. The non-Keplerian dynamics must quickly modify these orbits such that the particle will not impact the surface within its first revolution. Fig. 1 shows the initial conditions from the grid discussed in Section 4 mapped to a subset of the initial orbit elements. For every set of initial conditions in orbit element space (or in position/velocity space), there are 22 cases for the different particle sizes, as particle size does not change the initial state. In any given subset of initial conditions, there can be more cases at the same combination of initial conditions, as multiple launch velocities can lead to common orbit elements. Thus Fig. 1 does not intend to quantify the outcomes, but indicates how the strongly non-Keplerian dynamics can result in very different evolutionary outcomes for the same or similar initial orbits.

357

358

359

360

361

362

363

364

365

366

367

368

Each simulated trajectory is grouped into one of four outcomes: suborbital, direct escape, escape, or orbital. A suborbital case is where the particle re-impacts the asteroid before passing through periaipse, thus completing less than one revolution. A direct escape case is where the particle escapes the system before passing through periaipse. Escape from the Benu system is defined by a particle reaching a distance of 35 km from Benu, which is roughly its Hill radius. An escape case is a particle that eventually escapes, but first passes through one or more periaipses. Finally, an orbital case is one which passes through one or more periaipses, and eventually either re-impacts with Benu or, in a small number of cases, continues orbiting for a full Benu year (437 days). These classifications roughly correspond to the classification proposed by Scheeres et al. (2002): suborbitals are Class I; direct escapes are Class V; escapes are Class IV; and orbital cases encompass both Class II and III.

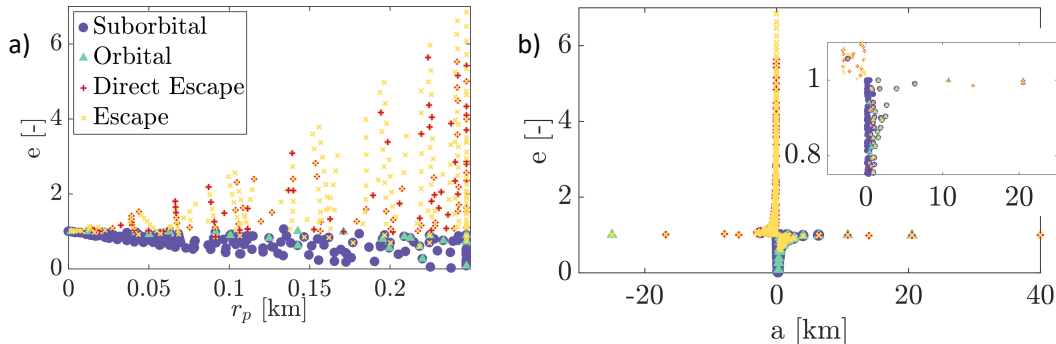


Figure 1. Initial orbit element relationships for simulated particles for the January 19 launch-site. Four symbols indicate the fate of particle from that initial condition. Panel a) shows eccentricity vs periaipse radius (which are at or below the surface of Benu, by definition), b) shows the eccentricity vs semimajor axis, and c) shows a zoomed-in portion of b) containing the majority of the orbital results.

369

370

371

372

373

374

375

376

There are several interesting conclusions to be drawn from Fig. 1. First, many particles that are launched on what should be hyperbolic orbits ($e > 1$ and/or $a < 0$) do not escape immediately. Most escape eventually, but they often come back toward Benu before escaping. These particles are usually launched toward the Sun, and SRP has enough time and strength to reverse the direction of motion such that the particles return toward Benu and then fly by to a subsequent escape. Second, most particles that are launched with $e < 1$ are suborbital and do not make it past their first periaipse; however, the orbital cases can begin with a wide variety of semimajor axes and very low periaipse radii

377 (all cases pictured have periape radii less than the equatorial radius of Bennu) – indi-
 378 cating that the non-Keplerian dynamics can greatly change the trajectory to prevent im-
 379 mediate re-impact. The suborbital fate likewise dominates the low-energy (small a) tra-
 380 jectories, as would be expected. A third observation is that there are some cases where
 381 particles launched on very high trajectories ($a \simeq \pm 20$ km) enter orbit. These trajec-
 382 tories also typically move toward the Sun, which allows SRP to remove a significant por-
 383 tion of their orbital energy such that they can be in a lower energy state upon their first
 384 periape passage.

385 To further demonstrate the non-Keplerian environment experienced by the parti-
 386 cles, Figs. 2 and 3 show time histories of the orbits and orbit elements for two particles
 387 that remained in orbit for the maximum simulation length of one Bennu year. These two
 388 particles had the same launch velocities – magnitude of 24 cm/s, azimuth of 150° , and
 389 elevation of 45° and differed only in their sizes, which were radii of 5 and 7 cm. The rapid
 390 variations in the orbit elements over the course of the year illustrate the complex dynam-
 391 ical environment.

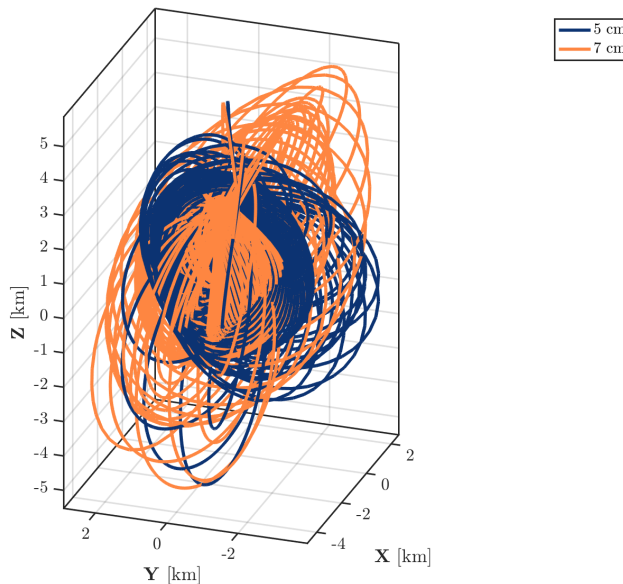


Figure 2. Simulated orbits of two particles with radii of 5 and 7 cm that temporarily remain in the Bennu environment. Particles initialized at the Jan 19 launchsite.

392 5.2 Population Evolution

393 A grid study such as is presented here is best used to understand the general be-
 394 havior of the overall populations of ejected particles. To this end, we wish to understand
 395 how the population for each ejection event evolves with time. It is of particular inter-
 396 est to understand what portions of the initial conditions lead to the four fates discussed
 397 in the previous section. This is pictured for one event in Fig. 4; the other simulated events
 398 follow very similar trends. The population quickly drops with nearly half of the parti-
 399 cles re-impacting the surface of Bennu within the first day, most of which are the sub-
 400 orbital cases. Interestingly, all direct escape cases last more than one day, meaning it takes
 401 at least that long for any particle to reach the Hill sphere. Most of the population has
 402 either re-impacted or escaped within 10 days. However, there is a small subset of the pop-

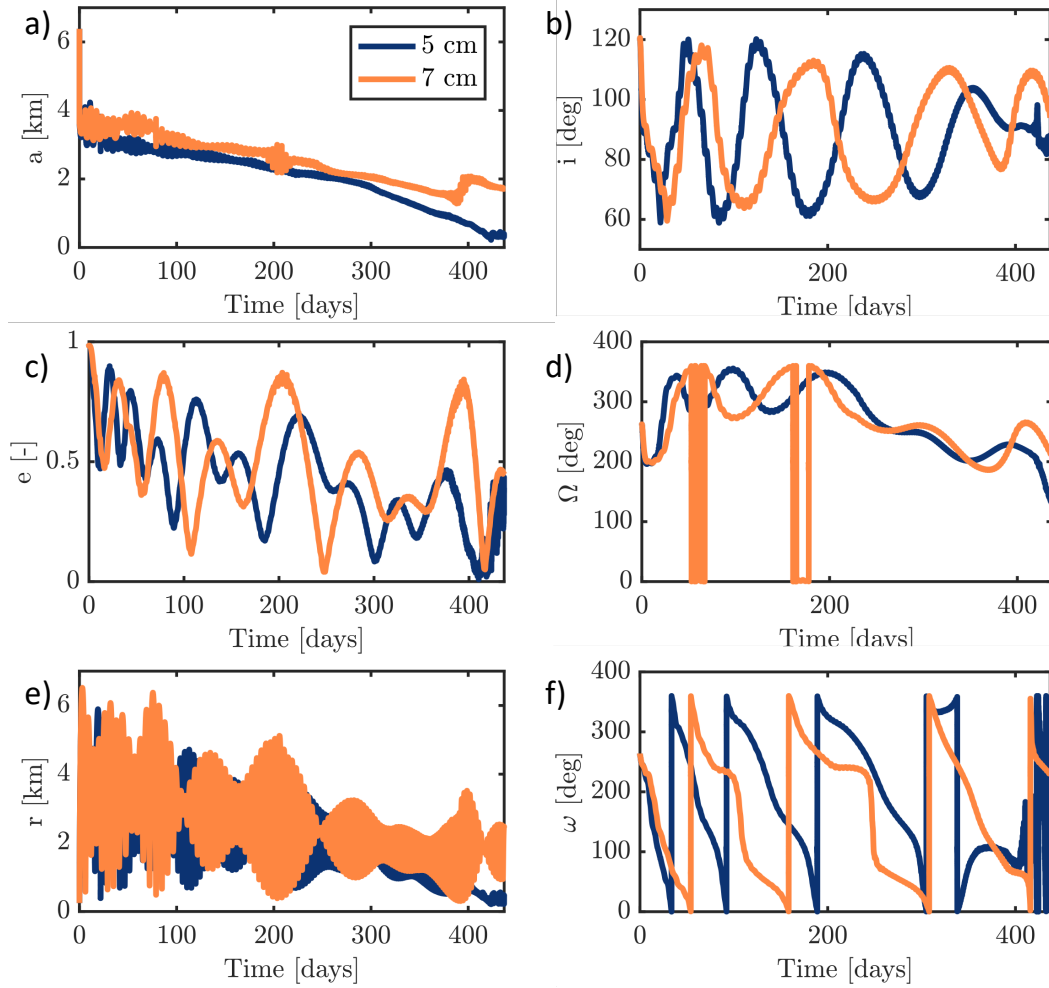


Figure 3. Keplerian orbit element evolution for the two particles shown in Fig. 2. Panel a) semimajor axis; b) inclination; c) eccentricity; d) right ascension of the ascending node; e) radius; and f) argument of periape.

403 uation which survives for much longer. Even a finite number of direct escape cases re-
 404 main within the Hill sphere for nearly 50 days. In this set of 17,666 particles, approx-
 405 imately 20 particles survive between 50 and 437 days, with 10 particles still in orbit af-
 406 ter one Bennu year.

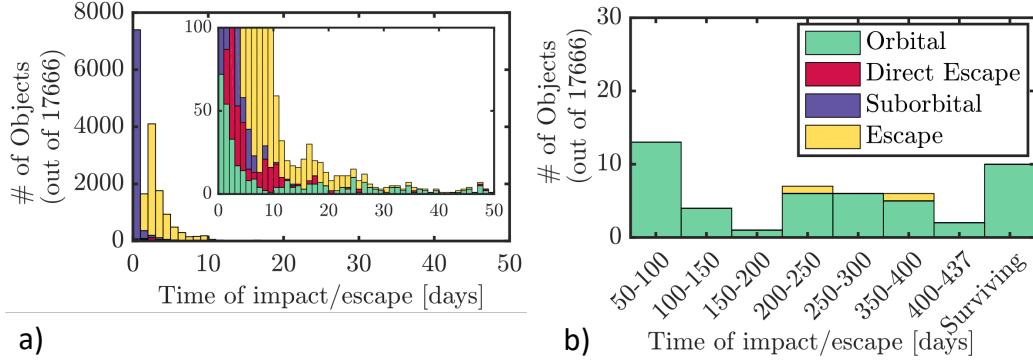


Figure 4. Simulated population evolution for the January 6, Site A case. Panel a) shows the total population for the first 50 days, with the inset zoomed in on a maximum of 100 particles. Panel b) shows the extended period for the remainder of a Bennu year.

407 One important aspect to understand about the particle lifetime is where the par-
 408 ticles exist at a given time. To first order, Fig. 5 answers this question by showing how
 409 many particles survive in a given radius band for the first 10 days after an ejection event.
 410 The population is grouped into three radii groups: < 1 km, which is the near-surface
 411 environment; 1 to 5 km, which, for OSIRIS-REx, is of particular interest because this
 412 is where the spacecraft operates for most of the mission; and finally 5+ km. The final
 413 line shown is the rest of the population, which has already returned to the surface or es-
 414 caped. This plot is very similar for all four ejection events. It shows that the near-surface
 415 environment quickly loses most of its population, with less than 1% of particles spend-
 416 ing time in this region after 1 day. The mid-radius region also reaches 1% after around
 417 2 days. More than 95% of particles re-impact or escape after 10 days. Finally, many sim-
 418 ulated particles reside for long periods of time at high altitudes with respect to the as-
 419 teroid; roughly half of the particles are beyond 5 km from Bennu 1 to 2 days after the
 420 ejection event, with many taking several more days to either escape or return to the sur-
 421 face. The population is not restricted to low altitudes.

422 Fig. 6 shows the relationship between launch velocity, area-to-mass ratio, particle
 423 size, and particle energy to the probability of escape. This figure demonstrates why we
 424 limited the grid search to be between 10 and 30 cm/s; all particles below 10 cm/s return
 425 to the surface, while all above 30 cm/s escape. Three main results can be drawn from
 426 these relationships. First, all particle sizes and area-to-mass ratios tested have a higher
 427 probability of escaping the system than re-impacting, but this is especially true for sub-
 428 centimeter particles. SRP can quickly add significant energy to these small particles, caus-
 429 ing them to escape from lower initial velocities and energies. Second, and unsurprisingly,
 430 the latitude of the ejection event site plays an important role in the chance of escape;
 431 the lower-latitude events provide more velocity to the particles from Bennu’s spin, and
 432 thus particles at lower launch velocities can escape, but also those at higher velocities
 433 launched westward move slower and do not escape. Third, the relationship with launch
 434 energy is interesting because there is a sweet spot in terms of maximizing the chance to
 435 re-impact. The lowest energies are associated with the smallest particles (due to their
 436 small mass) and thus they predominantly escape, while the largest energies also mostly

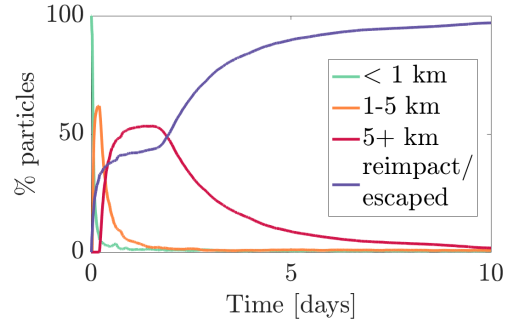


Figure 5. Percentage of population at various radii from the center of Bennu for the first 10 days after the January 6, Site A launchsite simulation.

437 escape due to the fact that they are launched at the highest velocities. In between, the
 438 interplay between mass, velocity, and launch geometry makes for a non-monotonic re-
 439 lationship.

440 5.3 Mass Migration

441 From a geophysical perspective, the most important aspect of the dynamics of ejected
 442 particles pertains to the particles that re-impact the surface. Where do they go? Is their
 443 distribution random? We gain insight into these questions through mapping the simu-
 444 lated re-impact locations from the four ejection event scenarios that we modeled, as shown
 445 in Figs. 7 and 8, where the re-impact locations for each event are binned by latitude and
 446 longitude over the surface of Bennu.

447 The highest concentration location in each case is roughly west of the launch sites.
 448 This corresponds to a large number of suborbital particles that do not leave the surface
 449 for very long, simply letting Bennu rotate under them for some period before coming back
 450 to the surface. Not all suborbital particles follow this pattern, however, as some can reach
 451 high altitudes above the surface before coming back down, allowing much more move-
 452 ment. Next, in terms of longitude, although each individual event displays some pref-
 453 erences, the pattern is not systematic across all event scenarios tested. This makes sense:
 454 as with the high suborbital cases, the particles that enter orbit for a finite period of time
 455 can have their orbits drastically changed, and, along with the variable lifetime, this al-
 456 lows these particles to land at random longitudes. It is noted that there are not strong
 457 patterns in terms of the local time at landing, other than the fact that the short period
 458 suborbital particles land within a few hours of the ejection local time. Longer lived par-
 459 ticles can land at a random local time given their assorted longitudes and lifetimes.

460 Latitude, however, is different. There is clearly an overall excess of ejection condi-
 461 tions that lead to re-impact at low latitudes. The January 19 and February 11 cases
 462 show a strong concentration near the equator. The January 6 cases are not concentrated
 463 as strongly near the poles, but still show a bias in landing locations at lower latitudes
 464 than their launch locations. This can be explained by the shape of Bennu, whose radius
 465 is largest near the equator and tapers toward the poles, and therefore has a higher chance
 466 of catching a particle at a low portion of its trajectory in this region. Overall, the re-impacting
 467 particles appear to be migrating toward the equator.

468 The results shown in Figs. 7 and 8 were totaled over all launch conditions to ob-
 469 tain a global view of the outcomes from a uniform ejection event. However, given the
 470 uncertainty surrounding the detailed physics of the ejection process creating the initial

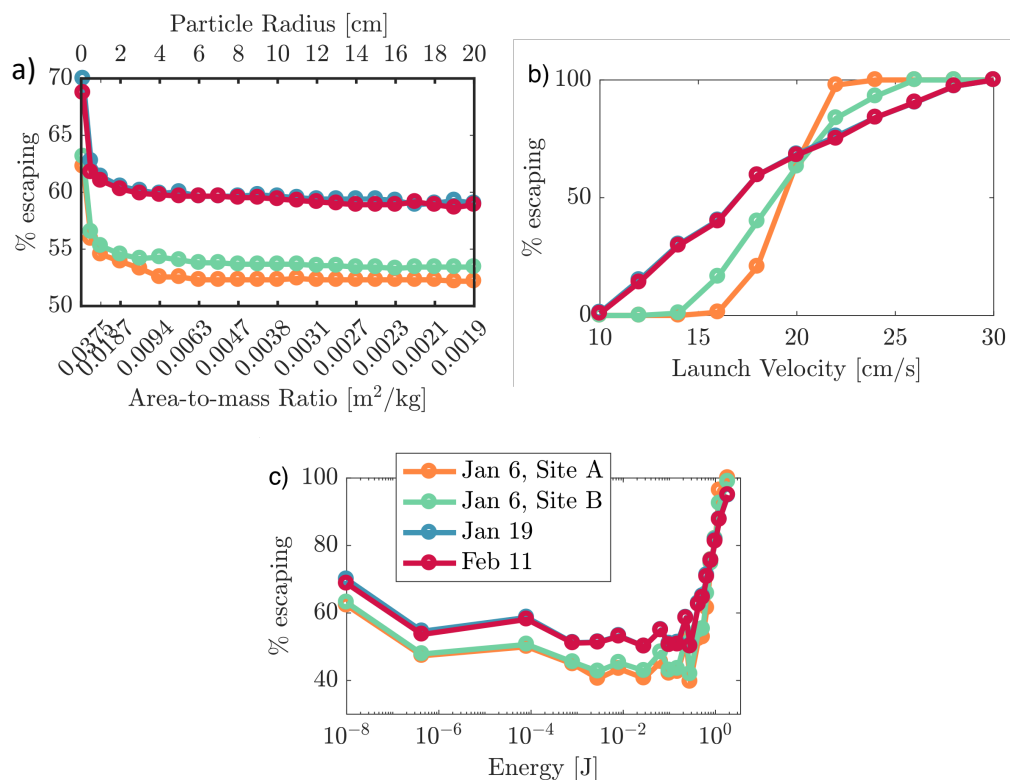


Figure 6. Percentage of population that escapes the system as a function of a) particle radius/area-to-mass ratio, b) launch velocity, and c) launch kinetic energy.

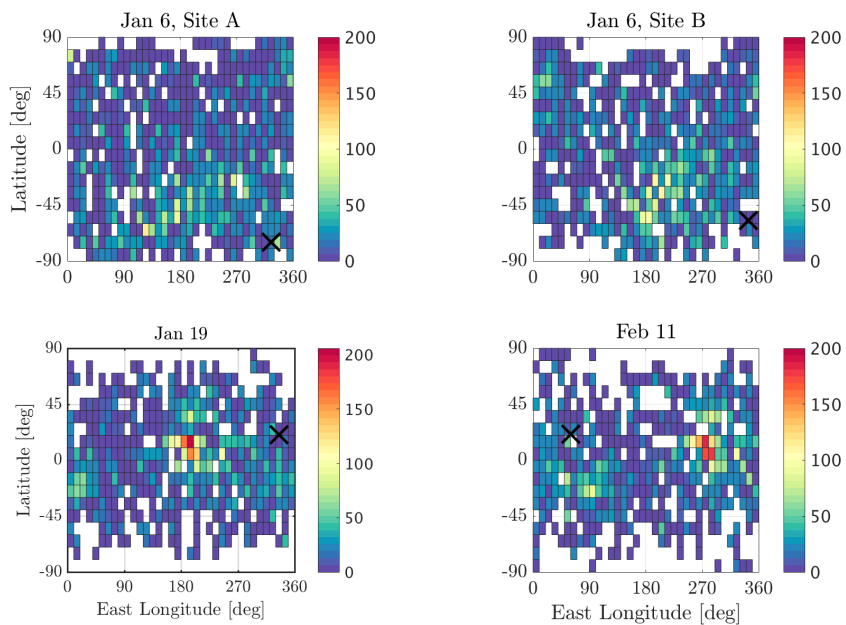


Figure 7. Re-impact locations for each simulated event, with number of particles (indicated by colorbar) binned in 10° by 10° latitude-longitude bins. Launch sites are marked with a black X.

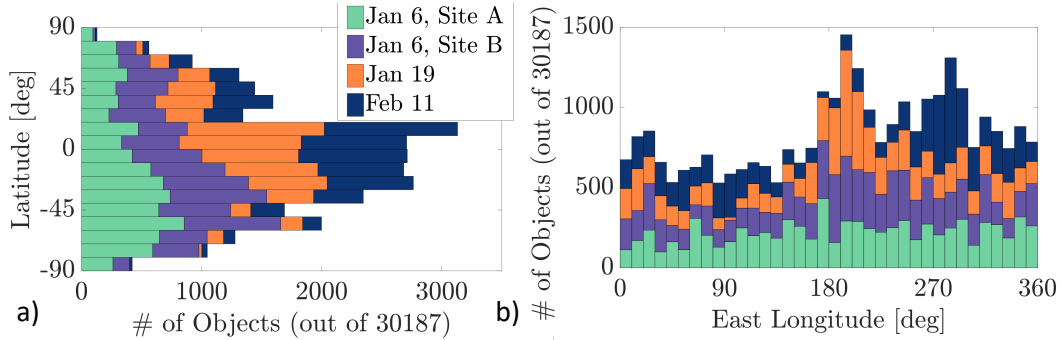


Figure 8. Re-impact locations for each simulated event, a) binned in 10° latitude bins, and b) binned in 10° longitude bins.

471 velocities (D. S. Lauretta et al., 2019), there could be a preferential direction of launch.
 472 To initially investigate this, we study two cases: an azimuthal preference versus an el-
 473 evation preference for the launch velocity.

474 In the azimuthal study, the launch velocity directions are defined in cones, such that
 475 all initial velocities projected onto the facet are within $\pm 45^\circ$ of the local cardinal direc-
 476 tion included in that case – north, south, east, or west. The results of this study for one
 477 ejection event are shown in Fig. 9 and 10. We note a longitudinal preference in re-impact
 478 locations between the different cases, with the East and North cases favoring a westward
 479 location, the West cases moving even further westward to include the opposite side of
 480 the body, and the South cases wrapping around and covering the eastward motion. We
 481 again see a trend of particles moving to lower latitudes – while this may be expected for
 482 such a high-latitude launch site, it was already shown in Fig. 8 that lower latitude launch
 483 sites are even more strongly biased toward low latitude landings. This result is interest-
 484 ing because regardless of the direction, much of the material ends up downhill of the ejection
 485 site, even if it does not reach the equator (see (Scheeres et al., 2019) for details of
 486 Bennu’s low-latitude region being at a lower potential than higher latitudes). It is also
 487 noteworthy in Figs. 9 and 10 that the eastward cases appear to follow a ground-track-
 488 type pattern with a maximum latitude around that of the launch site, which reinforces
 489 the fact that cases launched to the East are more likely to enter orbits that precess for
 490 some period before re-impacting than those launched in other directions.

491 In the elevation study, the cases are put into three bins: near horizontal ($< 30^\circ$),
 492 near vertical ($> 60^\circ$), and mid elevation between those two. Results for the February
 493 11 case are shown in Figs. 11 and 12. Here we see that the near-vertical cases move the
 494 least in longitude, while the near-horizontal cases move the farthest. All three cases show
 495 a fairly strong bias toward landing near the equator, which is partly due to this ejection
 496 event starting near the equator. However, events starting in this region do not show a
 497 preference for migrating to higher latitudes.

498 6 Discussion

499 The simulation results presented in Section 5 demonstrate several interesting phe-
 500 nomena that may be taking place around Bennu based on the ejection events seen in early
 501 2019.

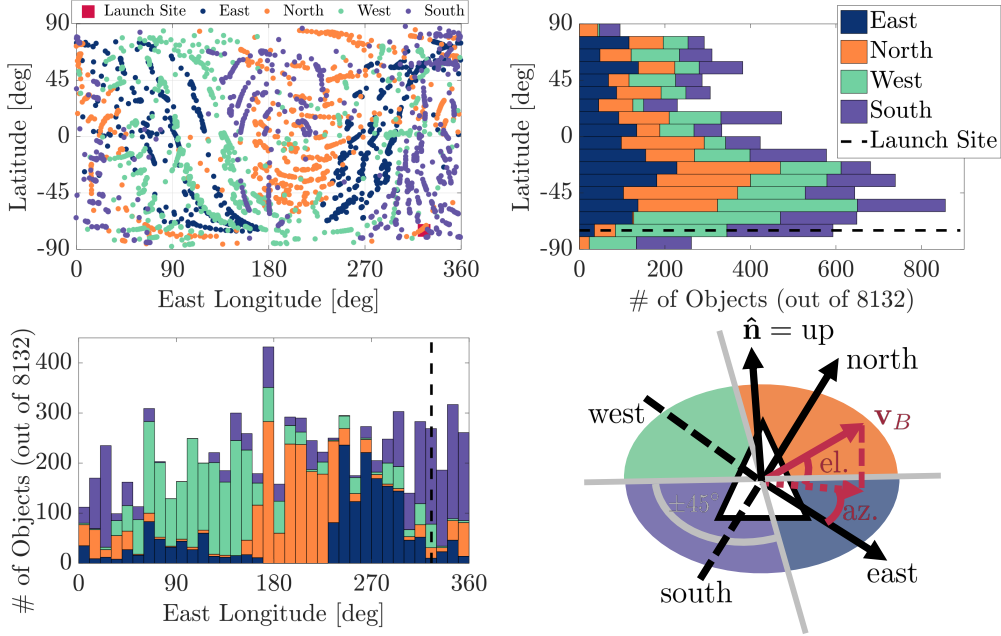


Figure 9. Map of the re-impact locations for the January 6, Site A launchsite case for the azimuthal direction sensitivity study, along with the associated latitude and longitude histograms. The sketch indicates how the four azimuth cases are determined by projecting the launch velocity into the facet plane – in this example this case falls within the east grouping.

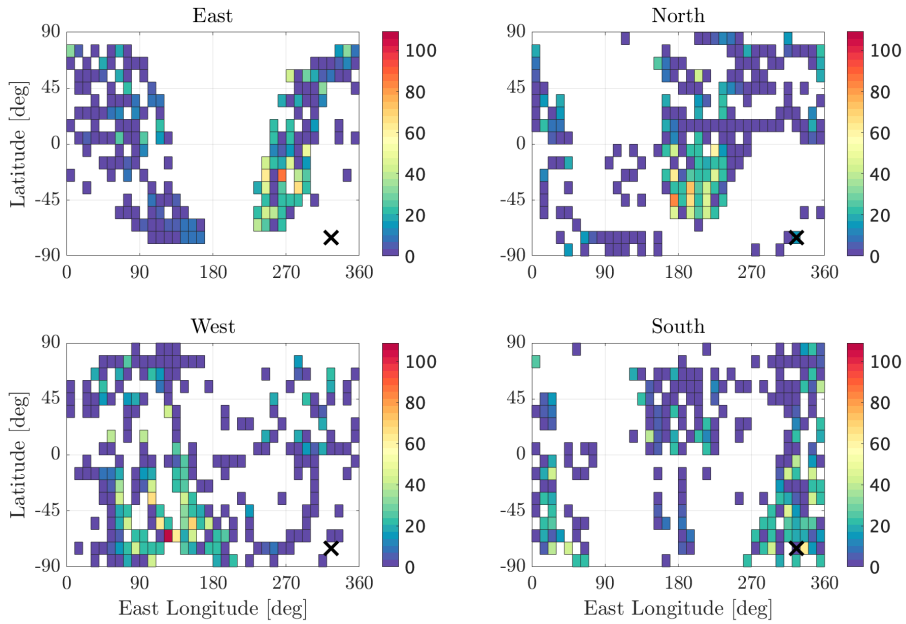


Figure 10. Re-impact locations for the January 6, Site A launchsite case for the azimuthal direction sensitivity study, with number of particles (indicated by colorbar) binned in 10° by 10° latitude-longitude bins.

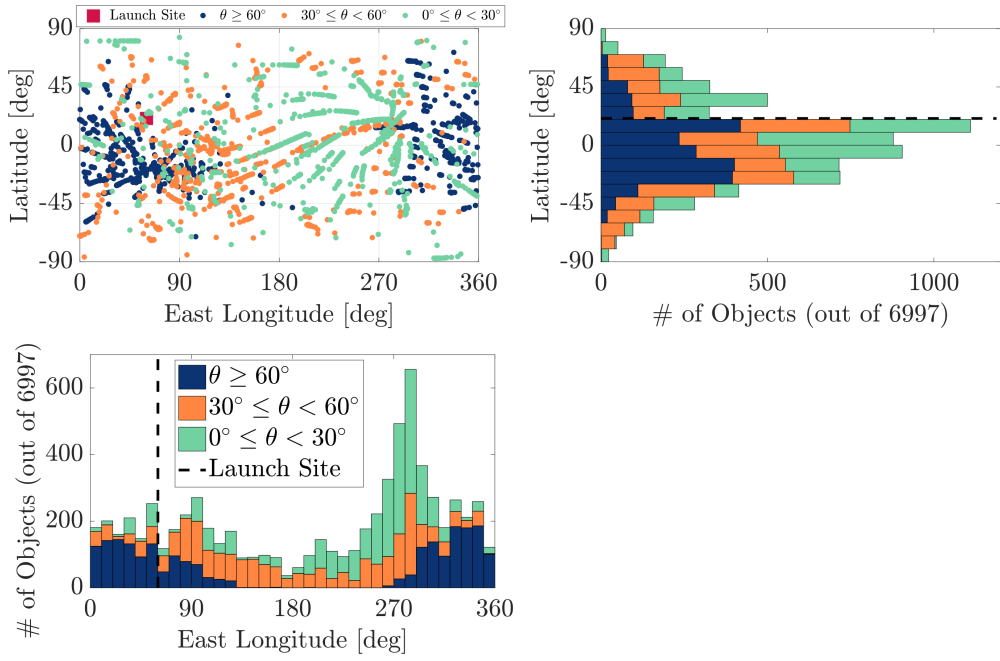


Figure 11. Map of the re-impact locations for the February 11 launchsite case for the elevation direction sensitivity study, along with the associated latitude and longitude histograms.

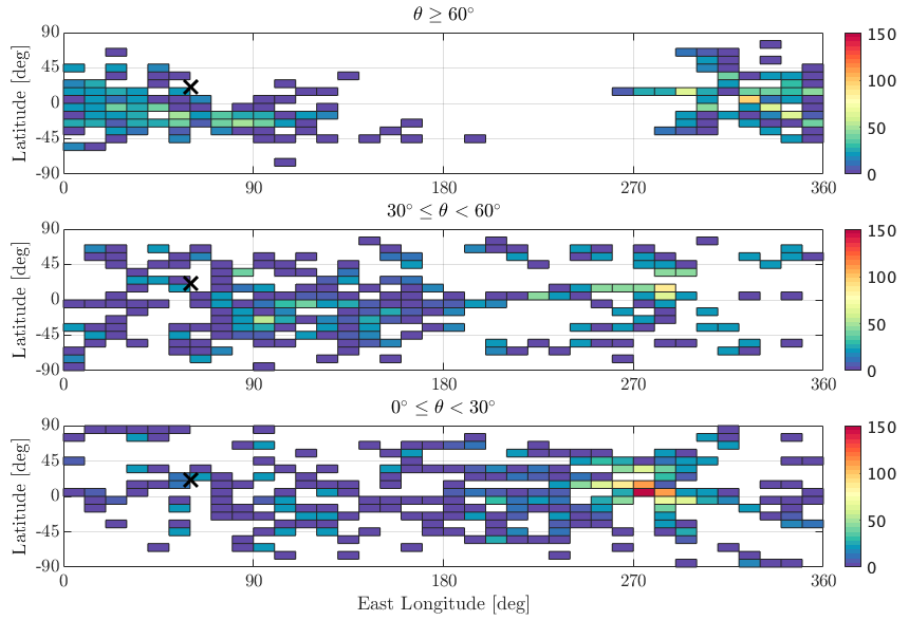


Figure 12. Re-impact locations for the February 11 launchsite case for the elevation direction sensitivity study, with number of particles (indicated by colorbar) binned in 10° by 10° latitude-longitude bins.

6.1 Observed Outcomes of the Simulated Populations

The combination of dynamical processes acting on ejected particles can result in many particles not only surviving for multiple revolutions, but potentially surviving for more than one heliocentric orbit around asteroids. The grid of initial conditions explored here was fairly rough and by no means exhaustive. Thus, the fact that conditions that lead to orbits that survive for multiple months exist in all four ejection scenarios studied here implies that there is a non-negligible chance for long-lived orbits to occur in nature. Depending on how regularly such ejection events take place, and how many particles are released at these events, it is possible that some particles are in orbit around Bennu for significant periods of time. The ejection of particles and their subsequent motion also allows for mass movement at small near-Earth asteroids both across the surface, and leaving the system.

The range of particles studied here indicates that, over our grid space, a given particle has a greater than even chance of escaping the system. Those odds dramatically increase for smaller particles with high area-to-mass ratios. This implies that when particles are ejected from the surface, there is a deficit of smaller particles among those that return to the surface. If the ejection process also plays a role in creating small particles, there may be a general lack of sub-centimeter particles on the surface of Bennu. Similarly, if the ejection process is lofting particles that already exist on the surface, then over time, this process could clean the surface of free, small particles. Overall, the population of small surface particles will depend on the relative rates of their creation, and subsequent removal through the ejection process.

These results also show that particles that return to re-impact the surface have significant mobility across the body. In all cases, re-impacting particles land preferentially at lower latitudes. A main reason for this is simply because Bennu has a larger radius near its equator. We do not consider here the dynamics of re-impact; however, it has already been established that the rotational Roche lobe for Bennu intersects the body around $\pm 20^\circ$ in latitude (Scheeres et al., 2019). Thus, particles that travel to this region are more likely to remain captured than those that re-impact at higher latitudes, which could further exacerbate the trend seen here. Importantly, this finding indicates that there could be a self-reinforcing mechanism at play: once an equatorial bulge is established, ejected material is more likely to land there, thus increasing the radius of the bulge (and if material is coming from higher latitudes, decreasing the radius there), thereby exaggerating the “top” shape. Detailed simulation investigating how such a process might work in coupling the change in shape with the dynamics of ejected particles will be explored in future work.

This mass movement also provides a previously unconsidered mechanism which can contribute to crater erasure, especially at lower latitudes. Landslides are thought to be the main mechanism for crater erasure (Miyamoto et al., 2007), which should leave evidence of directional mass motion. Erasing craters through in-fall of ejected particles may not leave such prominent directional evidence, given that material can come from a variety of directions based on the variety of orbits and trajectories that can be established. However, considering the preferential loss of smaller particles through ejection, craters filled in this manner should preferentially contain larger particle sizes.

6.2 Dynamical Implications

For an ejected particle to survive in orbit for more than one revolution, there must first be a mechanism to raise the particle’s periapse altitude before its first periapse passage. There are two ways to increase the periapse radius: either increase the semimajor axis (and thus the energy), or decrease the eccentricity.

551 The basis for understanding the rapid evolution of orbits around small bodies is
 552 given by Scheeres (2016), which accounts for the effects of the point mass gravity and
 553 SRP. That work shows that averaged over an orbit, SRP does not change the semimajor
 554 axis of an orbit, but it can change the eccentricity and the angular momentum in a
 555 coupled manner. Thus, SRP alone can increase survivability by lowering the eccentricity
 556 of some ejected particles. Furthermore, when a particle passes behind Bennu and is
 557 shadowed for some portion of its orbit, the SRP perturbation disappears. This changes
 558 the averaging results and can lead to a net gain in energy over these orbits.

559 However, Scheeres' theory can not fully explain all of our simulated results. Our
 560 simulations show that Scheeres' theory describes the main evolution of particle orbits
 561 that are far from the surface (on the order of 1 km and above), for periods where the
 562 semimajor axis does not vary substantially. However, at lower altitudes, the non-spherical
 563 gravity and TRP provide significant perturbations that cause different evolution. TRP,
 564 in particular, can cause significant perturbations during low altitude portions of the orbit,
 565 including at the initial stages of an orbit. The dominant component of the TRP acceleration
 566 is always in the radial direction away from the body, which can modify the eccentricity
 567 and, during some portions of an elliptical orbit, can lead to an energy change.
 568 Furthermore, because asteroids such as Bennu have a hot spot in the afternoon that is
 569 hottest at the equator, depending on the orientation of an orbit with respect to this hot
 570 region, there can be a net gain or loss in orbital energy as the particles fly past.

571 Beyond modifying the semimajor axis and eccentricity of the orbit, reorientation
 572 of the orbit plane and periapse location can also extend the orbital lifetime in two ways.
 573 First, if the location of periapse is moved to higher latitudes, the periapse altitude is increased
 574 because Bennu has a smaller radius at higher latitudes. Second, there can be a resonance
 575 between the precession of the orbit and the inertial precession of the thermal hot spot.
 576 The hot spot is always located at the same Bennu local time, but that location varies in
 577 inertial space as Bennu moves in its orbit about the Sun. If an orbit is oriented such that
 578 this hot spot adds energy through TRP, this relationship can be kept for many revolutions
 579 if the precession rates of the orbit line up appropriately. Orbital precession is caused by
 580 non-spherical gravity, 3rd body gravity, and SRP (and to a lesser degree by TRP); thus,
 581 there is a complicated coupling between the various dynamical processes that can lead to
 582 a higher periapse and a longer orbit.

583 It is also pertinent to point out how the dynamics affect the escape speed of ejected
 584 particles. It has previously been noted that due to the significant spin rates and the complex
 585 shapes of small asteroids, the escape speed is not constant over the surface of the
 586 asteroid as is the case for a planetary body (Scheeres, 2016). Escape speeds are higher
 587 from potential lows on the surface, and particles can more easily achieve the escape speed
 588 if they are launched in the direction of surface motion (to the east typically), whereas
 589 they would have to be launched faster relative to the surface to achieve escape when launched
 590 in the direction opposite surface motion. However, SRP makes this even more complex
 591 and dependent on the area-to-mass ratio of the particles. Standard results from the literature
 592 indicate that SRP does not change orbital energy of unshadowed orbits, but this argument
 593 is based on treating SRP as a small perturbation and performing orbital averaging (Scheeres,
 594 2016). In this scenario, these assumptions do not hold. Particles launched toward the Sun
 595 will lose energy, and thus may not escape even though they are launched with a velocity
 596 above the local escape speed, and vice versa for those launched away from the Sun.
 597 Particles that do not escape will often subsequently approach close to the surface where
 598 other perturbations are significant enough to interfere with the averaging process. These
 599 effects become more severe as the particle area-to-mass ratio increases.

600 In short, a small asteroid ejecting particles is a rich and complex dynamical environment,
 601 and we have only explained some of the main mechanisms here. A detailed discussion and
 602 theoretical derivation to build upon current theories will be left to future work.
 603

6.3 Limitations of the Presented Study

While our inferences are well supported by the simulations presented in this work, further investigation should be carried out to ensure these results are robust given the assumptions that have been made. Care should be taken in extrapolating these results for statistical interpretations because they are conditioned on a uniform grid across the input parameters. Furthermore, the population statistics presented here may be skewed by the range of parameters used, in particular with regard to particle size, which could exist at smaller sizes than we simulated. The simulations also only investigated particle dynamics associated with the three observed ejection events (four possible ejection sites) documented in D. S. Lauretta et al. (2019), which share a late afternoon local time of launch and occurred relatively close to Bennu’s perihelion. Finally, our simulated populations do not include very slow or very fast particles, which will clearly produce sub-orbital and direct escape trajectories, respectively. Therefore, in order to apply the results here in a statistical sense based on some distribution of launch conditions, the results must be weighted accordingly to account for particles outside the range used here.

Several other dynamical effects may be acting on these particles that are not included here. In particular, the particles could be shedding mass or outgassing after their release, creating an effective thrust and possibly changing their area-to-mass ratio over time (Clark et al., 2004). Treating the particles as effective spheres for SRP and TRP modeling may also be inaccurate, and accommodations for the time-varying effects of a rotating flat plate may result in SRP acting in a slightly different direction, which would influence the results (Rosengren & Scheeres, 2014). Electrostatic forces are also not considered here, but could be important near the surface (C. M. Hartzell & Scheeres, 2013; C. Hartzell et al., In Review), effectively modifying the launch conditions, what happens on low-altitude periapse passages, and the details of the landing locations. Finally, gas drag could play an important role at low altitudes, although the navigation team has determined it is insignificant at 1 km radius (Geeraert et al., 2019). Further investigation of these effects is warranted in the future.

7 Conclusion

We simulated the dynamical evolution of populations of particles similar to those that were ejected from Bennu in events observed by OSIRIS-REx in early 2019. We showed that the combined effects of gravity, solar radiation pressure, and thermal radiation pressure from Bennu can cause the orbits of many simulated particles to last for months or longer. Furthermore, the simulated populations exhibit two interesting phenomena that could play an important role in the geophysical evolution of bodies such as Bennu. First, small particles (< 1 cm radius) are preferentially removed from the system, which could lead to a deficit of such particles on the surface. Second, re-impacting particles preferentially land near or on the equatorial bulge of Bennu. Over time, this can lead to crater in-filling and growth of the equatorial radius without requiring landslides.

Acknowledgments

We are grateful to the entire OSIRIS-REx team for making the encounter with Bennu possible. This material is based upon work supported by NASA under Contract NNM10AA11C issued through the New Frontiers Program. A portion of this work was conducted at the Jet Propulsion Laboratory, California Institute of Technology under a contract with the National Aeronautics and Space Administration. NavCam 1 image data will be available via the Planetary Data System (PDS) (<https://sbn.psi.edu/pds/resource/orex/>). BR acknowledges funding support from the Royal Astronomical Society (RAS) and the UK Science and Technologies Facilities Council (STFC). Simulation code used to generate these results and generated data are available online at https://github.com/cephid13/BennuParticles_JGR2019.git (McMahon, 2020).

654

References

655

Arakawa, M., Wada, K., Saiki, T., Kadono, T., Takagi, Y., Shirai, K., . . . Sawada, H. (2017, Jul 1). Scientific objectives of small carry-on impactor (sci) and

656

deployable camera 3 digital (dcam3-d): Observation of an ejecta curtain and a crater formed on the surface of ryugu by an artificial high-velocity impact.

657

Space Science Reviews, 208(1), 187–212. Retrieved from <https://doi.org/10.1007/s11214-016-0290-z> doi: 10.1007/s11214-016-0290-z

658

659

660

Barnouin, O., Daly, M., Palmer, E., Gaskell, R., Weirich, J., Johnson, C., . . . others (2019). Shape of (101955) bennu indicative of a rubble pile with internal stiffness. *Nature geoscience*, 12(4), 247.

661

662

663

Broschart, S. B., Lantoine, G., & Grebow, D. J. (2014). Quasi-terminator orbits near primitive bodies. *Celestial Mechanics and Dynamical Astronomy*, 120(2), 195–215.

664

665

666

Broschart, S. B., Scheeres, D., & Villac, B. F. (2009). New families of multi-revolution terminator orbits near small bodies. *Advances in the Astronautical Sciences*, 135(3), 1685–1702.

667

668

669

Clark, B., Green, S., Economou, T., Sandford, S., Zolensky, M., McBride, N., & Brownlee, D. (2004). Release and fragmentation of aggregates to produce heterogeneous, lumpy coma streams. *Journal of Geophysical Research: Planets*, 109(E12).

670

671

672

673

DellaGiustina, D., Emery, J., Golish, D., Rozitis, B., Bennett, C., Burke, K., . . . others (2019). Properties of rubble-pile asteroid (101955) bennu from osiris-rex imaging and thermal analysis. *Nature Astronomy*, 3(4), 341.

674

675

676

Garcia Yarnoz, D., Sanchez Cuartielles, J.-P., & McInnes, C. R. (2014). Passive sorting of asteroid material using solar radiation pressure. *Journal of Guidance, Control, and Dynamics*, 37(4), 1223–1235.

677

678

679

Geeraert, J. L., Leonard, J. M., Kenneally, P., Antreasian, P. G., Moreau, M. C., & Lauretta, D. S. (2019). Osiris-rex navigation small force models. In *Proceedings of the 2019 aas/aiaa astrodynamics specialist conference*.

680

681

682

Geissler, P., Petit, J.-M., Durda, D. D., Greenberg, R., Bottke, W., Nolan, M., & Moore, J. (1996). Erosion and ejecta reaccretion on 243 ida and its moon. *Icarus*, 120(1), 140–157.

683

684

685

Giancotti, M., Campagnola, S., Tsuda, Y., & Kawaguchi, J. (2014). Families of periodic orbits in hills problem with solar radiation pressure: application to hayabusa 2. *Celestial Mechanics and Dynamical Astronomy*, 120(3), 269–286.

686

687

688

Hamilton, V., Simon, A., Christensen, P., Reuter, D., Clark, B., Barucci, M., . . . others (2019). Evidence for widespread hydrated minerals on asteroid (101955) bennu. *Nature Astronomy*, 3(4), 332.

689

690

691

Hartzell, C., Zimmerman, M., Hergenrother, D., & DS, L. (In Review). An evaluation of electrostatic lofting as an active mechanism on bennu. *Journal of Geophysical Research: Planets*, TBD(TBD).

692

693

694

Hartzell, C. M., & Scheeres, D. (2013). Dynamics of levitating dust particles near asteroids and the moon. *Journal of Geophysical Research: Planets*, 118(1), 116–125.

695

696

697

Hergenrother, C. W., Maleszewski, C. K., Nolan, M. C., Li, J. Y., Drouet d’Aubigny, C. Y., Shelly, F. C., . . . Team, T. O.-R. (2019). The operational environment and rotational acceleration of asteroid (101955) Bennu from OSIRIS-REx observations. *Nature Communications*, 10(1), 1291.

698

699

700

701

Hesar, S. G., Scheeres, D., McMahon, J. W., & Rozitis, B. (2017). Precise model for small-body thermal radiation pressure acting on spacecraft. *Journal of Guidance, Control, and Dynamics*, 40(10), 2432–2441.

702

703

704

Korycansky, D., & Asphaug, E. (2004). Simulations of impact ejecta and regolith accumulation on asteroid eros. *Icarus*, 171(1), 110–119.

705

706

707

708

Lantukh, D., Russell, R. P., & Broschart, S. (2015). Heliotropic orbits at oblate asteroids: balancing solar radiation pressure and j2 perturbations. *Celestial Me-*

- 709 *chanics and Dynamical Astronomy*, 121(2), 171–190.
- 710 Lauretta, D., DellaGiustina, D., Bennett, C., Golish, D., Becker, K., Balram-
711 Knutson, S., ... others (2019). The unexpected surface of asteroid (101955)
712 bennu. *Nature*, 568(7750), 55.
- 713 Lauretta, D. S., Hergenrother, C. W., Chesley, S. R., Leonard, J. M., Pelgrift, J. Y.,
714 Adam, C. D., ... Wolner, C. W. V. (2019). Episodes of particle ejection
715 from the surface of the active asteroid (101955) bennu. *Science*, 366(6470).
716 Retrieved from [https://science.sciencemag.org/content/366/6470/](https://science.sciencemag.org/content/366/6470/eaay3544)
717 [eaay3544](https://doi.org/10.1126/science.aay3544) doi: 10.1126/science.aay3544
- 718 Leonard, J. M., Geeraert, J. L., Page, B. R., French, A. S., Antreasian, P. G.,
719 Adam, C. D., ... Lauretta, D. S. (2019). Osiris-rex orbit determination per-
720 formance during the navigation campaign. In *Proceedings of the 2019 aas/aiaa*
721 *astrodynamics specialist conference*.
- 722 McMahan, J. (2020). *Bennuparticles_jgr2019*. Zenodo. Retrieved from [https://doi](https://doi.org/10.5281/zenodo.3606693)
723 [.org/10.5281/zenodo.3606693](https://doi.org/10.5281/zenodo.3606693) doi: 10.5281/zenodo.3606693
- 724 McMahan, J., Scheeres, D., Hesar, S., Farnocchia, D., Chesley, S., & Lauretta, D.
725 (2018). The osiris-rex radio science experiment at bennu. *Space Science*
726 *Reviews*, 214(1), 43.
- 727 Miyamoto, H., Yano, H., Scheeres, D., Abe, S., Barnouin-Jha, O., Cheng, A. F., ...
728 others (2007). Regolith migration and sorting on asteroid itokawa. *Science*,
729 316(5827), 1011–1014.
- 730 *Osiris-rex naif repository*. (2020). Retrieved from [https://naif.jpl.nasa.gov/](https://naif.jpl.nasa.gov/pub/naif/ORB/kernels/)
731 [pub/naif/ORB/kernels/](https://naif.jpl.nasa.gov/pub/naif/ORB/kernels/)
- 732 Rieger, S. M., Scheeres, D., & Barbee, B. (2018). Orbital stability regions for hy-
733 pothetical natural satellites of (101955) bennu. *Journal of Spacecraft and Rock-*
734 *ets*, 56(3), 789–800.
- 735 Rizk, B., Pajola, M., Walsh, K., Bierhaus, E., DellaGiustina, D., Drouet dAubigny,
736 C., ... the OSIRIS-REx Team. (2019). Exposed inclusions or fallback? a
737 closer look at bennus weathered boulders. In *Epsc-dps joint meeting*.
- 738 Rosengren, A. J., & Scheeres, D. (2014). On the milankovitch orbital elements for
739 perturbed keplerian motion. *Celestial Mechanics and Dynamical Astronomy*,
740 118(3), 197–220.
- 741 Rozitis, B., & Green, S. F. (2011). Directional characteristics of thermal-infrared
742 beaming from atmosphereless planetary surfaces - a new thermophysical
743 model. *Monthly Notices of the Royal Astronomical Society*, 415, 2042–2062.
- 744 Rozitis, B., & Green, S. F. (2012). The influence of rough surface thermal-infrared
745 beaming on the yarkovsky and yorp effects. *Monthly Notices of the Royal As-*
746 *tronomical Society*, 423, 367–388.
- 747 Rozitis, B., & Green, S. F. (2013). The influence of global self-heating on the
748 yarkovsky and yorp effects. *Monthly Notices of the Royal Astronomical Soci-*
749 *ety*, 433, 603–621.
- 750 Russell, R. P., Lantukh, D., & Broschart, S. B. (2016). Heliotropic orbits with zonal
751 gravity and shadow perturbations: Application at bennu. *Journal of Guidance,*
752 *Control, and Dynamics*, 1925–1933.
- 753 Scheeres, D. (2016). *Orbital motion in strongly perturbed environments: applications*
754 *to asteroid, comet and planetary satellite orbiters*. Springer.
- 755 Scheeres, D., Durda, D., & Geissler, P. (2002). The fate of asteroid ejecta. *Asteroids*
756 *III*, 527–544.
- 757 Scheeres, D., McMahan, J., French, A., Brack, D., Chesley, S., Farnocchia, D., ...
758 others (2019). The dynamic geophysical environment of (101955) bennu based
759 on osiris-rex measurements. *Nature Astronomy*, 3(4), 352.
- 760 Schwartz, S. R., Yu, Y., Michel, P., & Jutzi, M. (2016). Small-body deflection tech-
761 niques using spacecraft: Techniques in simulating the fate of ejecta. *Advances*
762 *in space research*, 57(8), 1832–1846.

- 763 Vetrisano, M., Celletti, A., & Pucacco, G. (2016). Asteroid debris: Temporary
764 capture and escape orbits. *International Journal of Non-Linear Mechanics*, *86*,
765 23–32.
- 766 Werner, R. A., & Scheeres, D. (1996). Exterior gravitation of a polyhedron derived
767 and compared with harmonic and mascon gravitation representations of as-
768 teroid 4769 castalia. *Celestial Mechanics and Dynamical Astronomy*, *65*(3),
769 313–344.
- 770 Yu, Y., & Michel, P. (2018). Ejecta cloud from the aida space project kinetic impact
771 on the secondary of a binary asteroid: Ii. fates and evolutionary dependencies.
772 *Icarus*, *312*, 128–144.
- 773 Yu, Y., Michel, P., Schwartz, S. R., Naidu, S. P., & Benner, L. A. (2017). Ejecta
774 cloud from the aida space project kinetic impact on the secondary of a bi-
775 nary asteroid: I. mechanical environment and dynamical model. *Icarus*, *282*,
776 313–325.